

# UCSF

## UC San Francisco Previously Published Works

### Title

Loss of microRNAs in pyramidal neurons leads to specific changes in inhibitory synaptic transmission in the prefrontal cortex

### Permalink

<https://escholarship.org/uc/item/5jj2r355>

### Journal

Molecular and Cellular Neuroscience, 50(3-4)

### ISSN

1044-7431

### Authors

Hsu, Ruby  
Schofield, Claude M  
Dela Cruz, Cassandra G  
[et al.](#)

### Publication Date

2012-07-01

### DOI

10.1016/j.mcn.2012.06.002

Peer reviewed

Published in final edited form as:

*Mol Cell Neurosci.* 2012 July 1; 50(3-4): 283–292. doi:10.1016/j.mcn.2012.06.002.

## Dgcr8 is required in pyramidal neurons for normal inhibitory synaptic function

Ruby Hsu<sup>a</sup>, Claude M Schofield<sup>a</sup>, Cassandra G Dela Cruz<sup>a</sup>, Dorothy M Jones-Davis<sup>b</sup>, Robert Blelloch<sup>c</sup>, and Erik M Ullian<sup>a</sup>

<sup>a</sup>Departments of Ophthalmology and Physiology, University of California, San Francisco, CA 94143 USA

<sup>b</sup>Department of Neurology, University of California, San Francisco, CA 94143 USA

<sup>c</sup>The Eli and Edythe Broad Center of Regenerative Medicine and Stem Cell Research, Center for Reproductive Sciences, and Department of Urology, University of California, San Francisco, San Francisco, CA 94143

### Abstract

MicroRNAs (miRNAs) are critical regulators of nervous system function, and in vivo knockout studies have demonstrated that miRNAs are necessary for multiple aspects of neuronal development and survival. However, the requirements of miRNA biogenesis in the formation and function of synapses in the cerebral cortex are only minimally understood. Here, we have generated and characterized a mouse line with a conditional neuronal deletion of *Dgcr8*, a miRNA biogenesis protein predicted to process miRNAs exclusively. Loss of *Dgcr8* in pyramidal neurons of the cortex results in a non-cell-autonomous reduction in parvalbumin interneurons in the prefrontal cortex, accompanied by a severe deficit in inhibitory synaptic transmission and a corresponding reduction of inhibitory synapses. Together, these results suggest a vital role for miRNAs in governing essential aspects of inhibitory transmission and interneuron development in the mammalian nervous system. These results may be relevant to human diseases such as schizophrenia, where both altered *Dgcr8* levels as well as aberrant inhibitory transmission in the prefrontal cortex have been postulated to contribute to the pathophysiology of the disease.

### Keywords

microRNA; *Dgcr8*; inhibitory synaptic transmission; parvalbumin interneurons; prefrontal cortex

### 1 Introduction

MicroRNAs (miRNAs) constitute a class of highly-conserved, ~22–24 nucleotide (nt) long non-coding RNAs that bind to the 3' untranslated region of target mRNA species, leading to translational repression or mRNA degradation (reviewed in Bartel, 2004). The classifications of miRNAs and other small non-coding RNAs have been determined conventionally by the sequential processing reactions that constitute their biogenic pathway

© 2012 Elsevier Inc. All rights reserved.

Corresponding Author: Ruby Hsu, hsur@vision.ucsf.edu, 415.476.7993 (phone), 415.476.0336 (fax). Departments of Ophthalmology and Physiology, University of California, San Francisco, 10 Koret Way, Room K240, San Francisco, CA, 94143.

**Publisher's Disclaimer:** This is a PDF file of an unedited manuscript that has been accepted for publication. As a service to our customers we are providing this early version of the manuscript. The manuscript will undergo copyediting, typesetting, and review of the resulting proof before it is published in its final citable form. Please note that during the production process errors may be discovered which could affect the content, and all legal disclaimers that apply to the journal pertain.

(reviewed in Cao et al., 2006; Kim, 2005). Canonical, or “classic,” miRNAs are generated by the double-stranded RNA-binding protein DiGeorge Critical Region Gene 8 (*Dgcr8*), which complexes with the RNase III enzyme Drosha to cleave initially long primary-miRNA transcripts into ~70 nt stem-loop precursor-miRNAs. These in turn are then cleaved by the RNase III endonuclease Dicer to produce 22–24 nt mature miRNAs.

In mammals, miRNAs are expressed in the brain (Krichevsky et al 2003; Sempere 2003; Miska 2004) where their abundance and powerful regulatory capabilities may have particular importance for controlling both homeostatic and dynamic aspects of neural function. Initial investigations of miRNA-dependent phenotypes in rodent brain have principally focused on characterizations of total miRNA knockdown via genetic ablation of Dicer. These *in vivo* and *in vitro* studies have ascribed critical roles for miRNAs in regulating developmental processes including neurogenesis, proliferation, cell fate determination, and survival (Cheng et al 2009; Shibata et al 2008; Davis et al 2008; De Pietri Tonelli 2008). These and other seminal reports have greatly advanced the miRNA field; however, recent studies now indicate that Dicer does not exclusively process miRNAs and in fact has important functions outside of the miRNA pathway. Consequently, some of the phenotypes associated with Dicer deletion could be attributable to its miRNA-independent effects, via pathways involving endogenous small interfering RNAs, non-canonical miRNAs, or Alu RNA elements (Babiarz et al., 2008; Kaneko et al., 2011; Shapiro et al., 2010). Because the RNase III enzyme Drosha has been reported to have a distinct role in pre-rRNA processing (Wu et al., 2000) *Dgcr8* may be the only protein within the processing pathway that is specific to miRNAs. Therefore, identifying the neuronal phenotypes associated with *Dgcr8* loss might be the only experimental paradigm capable of deconvoluting the specific roles of miRNAs within the brain. Moreover, the development of cortical microcircuitry and synaptic function remain almost entirely unexplored in this context.

In order to investigate these outstanding questions, we generated a novel mouse line with *Dgcr8* conditionally deleted from principal neurons of the cortex (*Dgcr8<sup>fl/fl</sup>; Cre*) using a Cre line driven by the NEX promoter (Goebbels et al., 2006). These mice presented with a dramatic phenotype, including ataxia, tremors and microencephaly. Analysis of synaptic currents onto *Dgcr8<sup>fl/fl</sup>; Cre* pyramidal neurons in the prefrontal cortex (PFC) revealed a strong decrease in the frequency of inhibitory postsynaptic currents (IPSCs). Coinciding with this deficit were selective reductions in parvalbumin interneuron numbers and perisomatic inhibitory synapses. Together, these findings demonstrate for the first time the consequences of conditional, specific miRNA loss in the mammalian cortex as well as reveal an important non-cell-autonomous role for miRNAs on inhibitory synaptic transmission and interneuron development.

## 2 Materials and Methods

### 2.1 Generation of conditional knockout mice

Conditional deletion mice were generated using a previously established line in which the third exon of *Dgcr8* was floxed (*Dgcr8<sup>fl/fl</sup>*) via targeted homologous recombination (Rao et al., 2009; Wang et al., 2007). Mice were maintained in a C57/B16 background and backcrossed at least 4 generations. *Dgcr8<sup>fl/fl</sup>* mice were crossed to a line expressing Cre under the endogenous NEX promoter, which is expressed nearly exclusively in pyramidal cells from the neocortex and hippocampus (Goebbels et al., 2006). A heterozygous mating scheme was used to maintain at least one wildtype copy of the NEX gene in all progeny. A tdTomato strain driven by the ubiquitous Rosa promoter followed by a loxP-flanked STOP cassette (*Rosa-LSL-tdTomato*, Jackson Labs) was also crossed to the *Dgcr8<sup>fl/fl</sup>; Cre* line. In this line, fluorescent tdTomato was expressed in all cells having undergone Cre

recombination; tdTomato could therefore be used as a reporter for Cre expression. All animals used in this study were *Dgcr8<sup>fl/fl</sup>;Cre* or *Dgcr8<sup>fl/fl</sup>* littermate controls. Animal procedures were performed according to protocols approved by the appropriate Institutional Animal Care and Use Committee under the federal and state regulations.

## 2.2 qRT-PCR

Total RNA was extracted from the PFC of P16-P17 mice using traditional Trizol methods. To evaluate gene expression, 100ng of total RNA was used to generate cDNA using the Taqman Reverse Transcription Kit (Applied Biosystems). qPCR was performed using SYBR GreenER qPCR SuperMix (Invitrogen) on a CFX96 Real-Time System and a C1000 Thermal Cycler (Bio-Rad). GAPDH was used as an internal control. To evaluate miRNA expression, 1µg of total RNA was reverse-transcribed using the Taqman MicroRNA Reverse Transcription Kit (Applied Biosystems). miRNA qPCR was performed using the Taqman Universal PCR Master Mix (Applied Biosystems) and custom-designed Taqman probes (IDT DNA) using techniques previously described (Tang et al., 2006). For sequences, see <http://urology.ucsf.edu/blellochlab/protocols.htm>. The U6 snRNA (ABI) was used as an internal control. All qPCR reactions were performed in triplicate and relative quantifications were calculated using the Pfaffl method (Pfaffl, 2001).

## 2.3 Anatomy and cellular analysis

For Nissl staining, brains were extracted from P16-P17 animals and fixed overnight in 4% paraformaldehyde (PFA) in 0.1 M phosphate buffer. After cryoprotection in 30% sucrose, 25 µm coronal sections were serially collected using a Leica CM1900 cryostat. Sections were stained using an aqueous chrome alum-gallocyanine method (Kiernan, 1990) and images were obtained at 2.5x magnification using an Olympus SZH10 microscope and at 10x using a Zeiss Axio Imager M1 fluorescent microscope. Anatomical measurements were evaluated using ImageJ software (Rasband, NIH). Cross sectional cortical thickness was measured across the primary somatosensory area at Bregma -0.08; brain diameter was measured at the widest point across at Bregma -0.08; and the cross-sectional area of the hippocampus was measured at Bregma -2.055. Prefrontal cortical measurements were taken at Bregma 1.545 (Bregma values are given for corresponding coronal sections in the wildtype based on anatomical landmarks). For Golgi staining, the FD Rapid Golgi stain Kit (FD Neurotechnologies) was performed according to the manufacturer's instructions. Sholl analyses were conducted on Golgi-impregnated sections using NeuronJ, a customized plug-in for ImageJ. Pyramidal neurons from the medial prefrontal cortex region were analyzed, and dendritic intersections were counted with a radius step size of 12 µm. TUNEL labeling was performed in PFC coronal sections using the FragEL DNA Detection Kit (Calbiochem) according to the manufacturer's instructions.

## 2.4 Chemoconvulsant-induced seizures

Prolonged seizures were induced in P17–18 *Dgcr8<sup>fl/fl</sup>;Cre* and *Dgcr8<sup>fl/fl</sup>* animals by intraperitoneal (IP) injection of pilocarpine (320 mg/kg, Sigma). Scopolamine methylnitrate (1 mg/kg, Sigma) was administered via IP injection 30 min prior to the pilocarpine injection to limit peripheral cholinergic effects. Mice were observed for at least 30 minutes after pilocarpine injection, and seizures were quantified by using the classification of Racine (1972). According to this classification, seizures are defined by facial automatisms, head and body tremors, forelimb clonus, rearing, and falling. Stage 3 is defined by the onset of forelimb clonus. The latency to the first stage 3 seizure after pilocarpine injection was recorded.

## 2.5 Electrophysiology

Prefrontal cortical slices were prepared from *Dgcr8<sup>fl/fl</sup>;Cre* and littermate control mice of either sex, age P15–17. Animals were anesthetized with isoflurane and decapitated, and the whole brain was removed and transferred into ice-cold cutting solution containing (in mM): 75 sucrose, 87 NaCl, 25 glucose, 25 NaHCO<sub>3</sub>, 2.5 KCl, 1.25 NaH<sub>2</sub>PO<sub>4</sub>, 10 MgSO<sub>4</sub>, and 0.5 CaCl<sub>2</sub>, equilibrated with 95% O<sub>2</sub>/5% CO<sub>2</sub>. Coronal sections 250–275 μm thick were cut on a vibratome and then transferred into a 33°C incubation chamber with artificial cerebral spinal fluid (ACSF) containing (in mM): 125 NaCl, 25 NaHCO<sub>3</sub>, 2.5 KCl, 1.25 NaH<sub>2</sub>PO<sub>4</sub>, 2 MgCl<sub>2</sub>, 1 CaCl<sub>2</sub>, and 10 glucose, equilibrated with 95% O<sub>2</sub>/5% CO<sub>2</sub> prior to recording. Whole-cell patch-clamp recordings were performed using a MultiClamp 700A amplifier (Molecular Devices) in a submerged bath recording chamber superfused with ACSF at a rate of 2 mL/minute. Recording electrodes were made of borosilicate glass and had a resistance of 2.5–4 MΩ when filled with intracellular solution, which contained (in mM): 135 CsCl, 10 HEPES, 10 EGTA, 5 QX-314 and 2 MgCl<sub>2</sub>. For recording IPSCs, cells were voltage clamped at –60 mV and the external ACSF contained 20 μM DNQX and 50 μM AP-5. For miniature IPSC (mIPSC) recordings 1 μM tetrodotoxin (TTX, Ascent Scientific) was included in the ACSF. For excitatory postsynaptic current (EPSC) and current-clamp recordings the intracellular solution contained (in mM): 110 K-gluconate, 20 KCl, 10 HEPES, 0.4 EGTA, 2 MgCl<sub>2</sub>; pH was 7.25 and osmolarity was adjusted to 280–290 mOsm with sucrose. During voltage clamp recordings, cells were clamped at –70 mV and IPSCs were blocked by bath application of the GABA-A receptor antagonist bicuculline methiodide (10 μM, Tocris). The liquid junction potential was 12.3 mV and corrected. Access resistance was monitored and cells were included for analysis only if the series resistance was <20 MΩ and the change of resistance was <25% over the course of the experiment. Data were acquired at 50 kHz using pClamp 10.2 (Molecular Devices) and filtered at 2 kHz.

## 2.6 Immunohistochemistry

P16–P17 animals were deeply anesthetized and transcardially perfused with saline followed by 4% PFA. Brains were then harvested, post-fixed, and cryoprotected in 30% sucrose. Coronal sections were collected at 20 μm using a Leica CM1900 cryostat. Staining was performed in phosphate buffer (PB) containing 0.2% Triton-X and 10% goat serum overnight at 4°C using antibodies against calretinin (1:3000, Millipore), somatostatin (1:250, Millipore), or parvalbumin (1:1000, Swant). AlexaFluor (Invitrogen) secondaries were used at 1:1000 for 1 hour. Sections were mounted using Vectashield with DAPI (Vector Labs) and imaged using a Zeiss Axio Imager M1 fluorescent microscope. To quantify cell number, ImageJ was used to count the absolute number of cells across all areas of a coronal slice taken at Bregma 1.545. In order to assess the integrity of cortical lamination, 40 μm sections were stained using the upper layer marker Cux1 (1:250 Santa Cruz) and the deeper layer marker Foxp2 (1:1000 AbCam). For staining of inhibitory synapses, a tissue slab containing the PFC was dissected on ice and lightly fixed in 2% PFA in 0.1 M PB for 20 minutes followed by cryoprotection in 30% sucrose. 20 μm coronal sections were stained against VGAT (1:1000, Synaptic Systems) and gephyrin (1:1000, Synaptic Systems) overnight at 4°C, followed by AlexaFluor secondary staining (1:1000). TrkB (1:1000 BD Biosciences) and PV co-staining was performed using the same light fixation technique. Sections were imaged on a LSM 5 Pascal Confocal microscope. Inhibitory synapses were quantified by counting the number of overlapping VGAT and gephyrin puncta and dividing by the total number of VGAT plus gephyrin puncta. To quantify perisomatic synapses, 15 μm-diameter circles were traced around DAPI-labeled nuclei and the number of overlapping puncta within the region was divided by the total number of overlapping puncta in the field of view.

## 2.7 Western blotting

Total PFC brain lysates were extracted from P16-P17 animals using a lysis buffer containing 150 mM NaCl, 50mM Tris pH = 8.0, 1% Triton-X 100 with complete protease inhibitors (Roche). 15 $\mu$ g of protein per well was loaded into a 10% Bis-Tris SDS-PAGE gel (Invitrogen) under denaturing conditions. Proteins were transferred to PVDF membranes (Millipore), blocked in TBS-T, and blotted against TrkB (1:1000, B.D. Biosciences), BDNF (1:500, courtesy of Xin-Fu Zhou (Zhou and Rush, 1996)), or actin (1:1000, Sigma) overnight at 4°C.

## 3 Results

### 3.1 Conditional deletion of *Dgcr8* results in microencephaly and decreased neuron size

In order to specifically remove miRNAs from principal neurons of the cortex, we generated a conditional *Dgcr8* knockout mouse line (*Dgcr8<sup>fl/fl</sup>;Cre*) by crossing a floxed *Dgcr8* allele mouse strain (Rao et al., 2009; Wang et al., 2007) to a mouse expressing Cre recombinase driven by the endogenous NEX promoter. In this line, Cre recombinase is expressed in post-mitotic cortical pyramidal neurons and is absent from GABAergic interneurons (Goebbels et al., 2006). To confirm loss of *Dgcr8* and miRNAs in the cortex, we performed quantitative real-time PCR on *Dgcr8* and on a select panel of miRNAs highly expressed in neurons using total RNA isolated from *Dgcr8<sup>fl/fl</sup>;Cre* and *Dgcr8<sup>fl/fl</sup>* controls. *Dgcr8* levels were reduced compared to controls, as expected ( $39 \pm 5\%$ ; *Dgcr8<sup>fl/fl</sup>* n = 7; *Dgcr8<sup>fl/fl</sup>;Cre* n = 6,  $p < 0.0005$ ), and we also observed significant reductions in miRNA levels in the *Dgcr8<sup>fl/fl</sup>;Cre* compared to controls (miR-23a:  $43 \pm 9\%$ ; miR-124:  $56 \pm 8\%$ , miR-132:  $87 \pm 2\%$ ; miR-134:  $41 \pm 9\%$ ; let-7c:  $24 \pm 12\%$ ; *Dgcr8<sup>fl/fl</sup>* n = 7; *Dgcr8<sup>fl/fl</sup>;Cre* n = 6,  $p < 0.05$ ; Supplemental Figure 1).

We initially evaluated the impact of *Dgcr8* loss on gross neuroanatomy by performing Nissl staining on control and *Dgcr8<sup>fl/fl</sup>;Cre* brains. Similar to previous findings in a conditional Dicer knockout (Davis et al., 2008), we found a dramatic reduction in brain diameter (*Dgcr8<sup>fl/fl</sup>* =  $8.67 \pm 0.79$  mm; *Dgcr8<sup>fl/fl</sup>;Cre* =  $5.83 \pm 0.08$  mm;  $p = 0.02$ ; Figure 1A), cortical thickness (*Dgcr8<sup>fl/fl</sup>* =  $1.33 \pm 0.06$  mm; *Dgcr8<sup>fl/fl</sup>;Cre* =  $0.56 \pm 0.04$  mm;  $p = 0.0003$ ; Figure 1A), and hippocampal size (*Dgcr8<sup>fl/fl</sup>* =  $2.36 \pm 0.34$  mm<sup>2</sup>; *Dgcr8<sup>fl/fl</sup>;Cre* =  $0.70 \pm 0.03$  mm<sup>2</sup>;  $p = 0.009$ ; n = 6 per genotype; example shown in Fig 1A). Frontal cortex measurements were also greatly reduced (parietal cortex: *Dgcr8<sup>fl/fl</sup>* =  $1.36 \pm 0.06$  mm; *Dgcr8<sup>fl/fl</sup>;Cre* =  $0.77 \pm 0.06$  mm;  $p < 0.0001$ ; frontal cortex: *Dgcr8<sup>fl/fl</sup>* =  $1.34 \pm 0.06$  mm; *Dgcr8<sup>fl/fl</sup>;Cre* =  $0.74 \pm 0.03$  mm;  $p < 0.0001$ ; cingulate cortex: *Dgcr8<sup>fl/fl</sup>* =  $1.54 \pm 0.05$  mm; *Dgcr8<sup>fl/fl</sup>;Cre* =  $0.83 \pm 0.04$  mm;  $p < 0.0001$ ; n = 6 per genotype; Figure 1B). To investigate whether the severe microencephaly was due to a failure of newly-born neurons to migrate to their proper cortical positions, we examined gross cortical layer organization using immunocytochemistry. Staining for upper (Cux1) and deeper (Foxp2) layer cortical markers showed that these layer positional identities were retained, suggesting overall intact lamination (n = 2 per genotype; Figure 1C).

We next sought to determine whether the cortical microencephaly was due to a reduction in cell number, a reduction of cell size, or both. First, cell density of the PFC region was evaluated by counting cells per  $\mu$ m<sup>2</sup>. An increase in cell density was observed in the *Dgcr8<sup>fl/fl</sup>;Cre* animals (*Dgcr8<sup>fl/fl</sup>* =  $16.1 \pm 0.6$  cells/100  $\mu$ m<sup>2</sup>; *Dgcr8<sup>fl/fl</sup>;Cre* =  $27.9 \pm 2.1$  cells/100  $\mu$ m<sup>2</sup>;  $p < 0.0001$ ; n = 6 per genotype). This was accompanied by an increase in cell death as revealed by TUNEL staining (n = 2 per genotype, Supplemental Figure 2) as well as a significant shrinkage in the average soma size (*Dgcr8<sup>fl/fl</sup>* =  $188.5 \pm 13.8$   $\mu$ m<sup>2</sup>; *Dgcr8<sup>fl/fl</sup>;Cre* =  $105.1 \pm 13.4$   $\mu$ m<sup>2</sup>;  $p < 0.001$ ; Figure 2A, B), demonstrating that both cell loss and a reduction in cell body size contribute to the loss in cortical thickness. Golgi staining of PFC neurons supported the finding of cell shrinkage, as neurons in the

*Dgcr8<sup>fl/fl</sup>;Cre* displayed reduced dendritic arborization, with only  $5.17 \pm 0.48$  basal dendrites per neuron compared to  $18.70 \pm 1.26$  in the controls ( $n = 30$  neurons from 4 animals per genotype,  $p < 0.001$ ). No differences were observed in the average length of dendrites (*Dgcr8<sup>fl/fl</sup>* =  $49.9 \pm 2.6$   $\mu\text{m}$ ; *Dgcr8<sup>fl/fl</sup>;Cre* =  $52.6 \pm 3.8$   $\mu\text{m}$ ; Figure 2B). Quantification by Sholl analysis confirmed a reduction in dendritic complexity in *Dgcr8<sup>fl/fl</sup>;Cre* neurons (Figure 2C). Together, these anatomical findings indicate that Dgcr8-dependent miRNA biogenesis is required for the proper morphogenesis of cerebral cortical neurons.

### 3.2 Conditional deletion of Dgcr8 results in increased susceptibility to spontaneous and chemoconvulsant-induced seizures

*Dgcr8<sup>fl/fl</sup>;Cre* mice display a severe behavioral phenotype, including claspings, ataxia and tremors (Supplemental Figure 3A), and they succumb to early postnatal lethality. To determine whether these phenotypes were accompanied by other neurological symptoms such as seizures, *Dgcr8<sup>fl/fl</sup>* and *Dgcr8<sup>fl/fl</sup>;Cre* mice were monitored for susceptibility to spontaneous and chemoconvulsant-induced seizures. Behavioral observation of *Dgcr8<sup>fl/fl</sup>;Cre* mice indicated a predisposition to spontaneous seizure activity induced by cage-handling stress; precautions were therefore taken to ensure minimal stress of the mice prior to seizure testing. Chemoconvulsant-induced seizures were provoked by IP injection of 320 mg/kg pilocarpine preceded 30 min by 1 mg/kg scopolamine methylnitrate. Seizures were provoked in both genotypes, but *Dgcr8<sup>fl/fl</sup>;Cre* mice exhibited a significantly shortened latency to stage 3 seizures as compared to their control littermates. *Dgcr8<sup>fl/fl</sup>* mice developed stage 3 seizures in  $14.15 \pm 3.23$  min ( $n = 5$ ), whereas *Dgcr8<sup>fl/fl</sup>;Cr* mice progressed to stage 3 seizures in  $5.31 \pm 0.67$  min ( $n = 6$ ;  $p = 0.016$ ; Supplemental Figure 3B).

### 3.3 Reduced inhibitory postsynaptic currents at Dgcr8<sup>fl/fl</sup>;Cre pyramidal neurons

Common forms of ataxia, seizures, and tremors are predicted to be primarily GABAergic in origin (Chiu et al., 2005). Accordingly, we hypothesized that there might be perturbations to inhibitory circuitry in the cortex of the conditional Dgcr8 knockout mice. To assess this, we performed whole-cell patch-clamp electrophysiological recordings on layer II/III pyramidal neurons in the PFC of *Dgcr8<sup>fl/fl</sup>* ( $n = 13$ ) and *Dgcr8<sup>fl/fl</sup>;Cre* mice ( $n = 13$ ; Figure 3) and examined pharmacologically isolated spontaneous IPSC events. Here, we found a profound reduction in the frequency of IPSCs in *Dgcr8<sup>fl/fl</sup>;Cre* mice (*Dgcr8<sup>fl/fl</sup>* =  $4.6 \pm 0.6$  Hz; *Dgcr8<sup>fl/fl</sup>;Cre* =  $1.0 \pm 0.2$  Hz;  $p < 0.0001$  Figure 3A, C). Coinciding with this deficit in frequency, the remaining events in *Dgcr8<sup>fl/fl</sup>;Cre* mice displayed a significant increase in IPSC amplitude (*Dgcr8<sup>fl/fl</sup>* =  $30 \pm 2$  pA; *Dgcr8<sup>fl/fl</sup>;Cre* =  $46 \pm 4$  pA;  $p = 0.002$ ; Figure 3A, C). The kinetics profiles of IPSC events were similar between genotypes (Figure 3B, C). Because alterations in IPSC frequency and amplitude can be attributable to changes in the action potential firing capabilities of presynaptic interneurons, we examined the mIPSC population by recording events in the presence of 1  $\mu\text{M}$  tetrodotoxin. Similar to the spontaneous data, we found a striking reduction in mIPSC event frequency (*Dgcr8<sup>fl/fl</sup>* =  $3.9 \pm 0.5$  Hz; *Dgcr8<sup>fl/fl</sup>;Cre* =  $0.6 \pm 0.1$  Hz;  $p < 0.0001$ ) and gain in mIPSC amplitude (*Dgcr8<sup>fl/fl</sup>* =  $24 \pm 1$  pA; *Dgcr8<sup>fl/fl</sup>;Cre* =  $30 \pm 2$  pA;  $p = 0.02$ ). Together, these data show that Dgcr8-dependent miRNA biogenesis is required for the normal development of inhibitory synaptic transmission, and pyramidal neurons deficient for Dgcr8 display a decrease in IPSC frequency that is accompanied by an increase in IPSC amplitude.

### 3.4 Perisomatic inhibitory synapses are reduced on Dgcr8 knockout pyramidal neurons

In order to determine whether changes in inhibitory synapse number could account for the changes in IPSC event frequency, we used immunohistochemical colocalization of the presynaptic vesicular GABA transporter (VGAT) and postsynaptic gephyrin to quantify the number of inhibitory synapses. Quantification of the percentage of colocalized pre- and post-synaptic puncta in the PFC revealed no significant differences between Dgcr8

knockouts and wildtypes, suggesting no change in the total number of inhibitory synapses in this region ( $Dgcr8^{fl/fl} = 11.8 \pm 1.2\%$ ,  $n = 3$  animals;  $Dgcr8^{fl/fl};Cre = 14.2 \pm 3.6\%$ ,  $n = 3$  animals; Figure 4A, B). However, certain classes of inhibitory neurons form a small percentage of the total number of synapses yet exert a powerful influence on inhibitory drive due to the localization and properties of these synapses (Markram et al., 2004; Miles et al., 1996). We therefore extended our examination to specifically quantify the inhibitory synapses surrounding the cell bodies. This analysis revealed a 25% decrease in the number of inhibitory synapses localized perisomatically ( $Dgcr8^{fl/fl} = 39.2 \pm 4.1\%$ ,  $n = 3$  animals;  $Dgcr8^{fl/fl};Cre = 29.4 \pm 2.1\%$ ,  $n = 3$  animals;  $p = 0.02$ ; Figure 4C). We therefore predict that this reduction in perisomatic inhibitory synapses can at least in part account for the reduction in IPSC frequency.

### 3.5 Selective loss of parvalbumin interneurons in the PFC of $Dgcr8$ conditional knockouts

In order to determine whether the changes in inhibitory transmission and the selective reduction of perisomatic inhibitory synapses could be attributed to a specific class of interneuron, the total population of calretinin (CR), somatostatin (SST), and parvalbumin (PV) subtypes was measured using immunohistochemistry. ~95% of all cortical interneurons can be accounted for using these three markers (Wonders and Anderson, 2006). CR immunostaining in the PFC revealed no significant changes in the absolute number of CR-positive cells ( $Dgcr8^{fl/fl} = 640 \pm 79$  cells;  $Dgcr8^{fl/fl};Cre = 667 \pm 33$  cells; Figure 5A). SST staining similarly showed no differences in absolute cell number ( $Dgcr8^{fl/fl} = 278 \pm 35$  cells;  $Dgcr8^{fl/fl};Cre = 284 \pm 39$  cells; Figure 5A). In contrast, when we examined the third class of interneurons, we found a dramatic reduction in the number of PV-positive cells in the  $Dgcr8^{fl/fl};Cre$  cortex ( $Dgcr8^{fl/fl} = 1182 \pm 204$  cells;  $Dgcr8^{fl/fl};Cre = 441 \pm 105$  cells;  $n = 3-4$  per genotype for all stainings;  $p = 0.01$ ; Figure 5A). Whereas the absolute number of CR and SST cells remained unchanged, the density of these cells increased, due to the smaller overall brain size (CR:  $Dgcr8^{fl/fl} = 57.1 \pm 9.3$  cells/mm<sup>2</sup>;  $Dgcr8^{fl/fl};Cre = 187.4 \pm 9.2$  cells/mm<sup>2</sup>;  $p < 0.001$ ; SST:  $Dgcr8^{fl/fl} = 12.1 \pm 1.1$  cells/mm<sup>2</sup>;  $Dgcr8^{fl/fl};Cre = 22.8 \pm 1.6$  cells/mm<sup>2</sup>;  $p < 0.001$ ; Figure 5B). The density of PV cells, however, remained unchanged in spite of the smaller brain size ( $81.0 \pm 9.6$  cells/mm<sup>2</sup>;  $Dgcr8^{fl/fl};Cre = 91.0 \pm 28.3$  cells/mm<sup>2</sup>;  $n = 3-4$  per genotype for all stainings; Figure 5B). To establish that the reduction of PV interneurons was not simply due to misexpression of the Cre recombinase outside of the NEX lineage, we crossed a *Rosa-LSL-tdTomato* reporter line to our recombinant strains. Staining for CR, SST, and PV showed no overlap with Cre reporter expression, which confirms the published expression of the NEX-Cre line (Goebbels et al., 2006) and indicates that the phenotypes observed were not due to Cre expression within these inhibitory cell types (Supplemental Figure 4). Together, these results demonstrate a selective loss of PV interneurons in the  $Dgcr8^{fl/fl};Cre$  PFC.

### 3.6 BDNF and TrkB expression are reduced in the $Dgcr8^{fl/fl};Cre$ PFC

Maturation of interneuron subclasses is regulated by a combination of intrinsic molecular programs and extrinsic signaling cues (Wonders and Anderson, 2006). For example, the development of PV interneurons is mediated by extrinsic signaling through the brain-derived neurotrophic factor (BDNF) and tropomyosin-related receptor tyrosine kinase B (TrkB) pathway (Eto et al., 2010; Patz et al., 2004; Wahle et al., 2000). To evaluate whether this pathway is altered in the  $Dgcr8^{fl/fl};Cre$  mice, Western blots were used to measure the levels of BDNF and TrkB expression in the PFC of  $Dgcr8^{fl/fl}$  and  $Dgcr8^{fl/fl};Cre$  animals. Significant reductions in both BDNF ( $37 \pm 3\%$ ,  $p = 0.01$ ) and TrkB protein ( $38 \pm 5\%$ ,  $p = 0.006$ ) were observed in the  $Dgcr8^{fl/fl};Cre$  when normalized to control values ( $n = 4$  per genotype; Figure 6A, B). Since TrkB is expressed in both pyramidal neurons and PV-positive interneurons, we evaluated the TrkB expression at the cellular level to determine what cells are responsible for the decrease in expression. Co-staining of TrkB and PV

revealed TrkB expression in the PV-positive interneurons in the *Dgcr8<sup>fl/fl</sup>;Cre* PFC (*Dgcr8<sup>fl/fl</sup>* = 30 cells; *Dgcr8<sup>fl/fl</sup>;Cre* = 33 cells; 2 animals per genotype; Figure 6C). The presence of TrkB in the PV cells that remain in the deletion animal is consistent with the fact that TrkB expression is required for normal PV interneuron development (Patz et al., 2004) and suggests that the cells which have reduced or lost TrkB expression fail to mature into PV interneurons. Additional studies examining the developmental time course of the TrkB loss will be required to resolve this point.

### 3.7 Additional electrophysiological characterization of PFC pyramidal neurons from control and Dgcr8 knockout mice

One alternative explanation for the phenotypes described by our data set is widespread cell death throughout the cortex accompanied by dysfunctional neurons. In order to rule this out as a major determining factor, we performed additional physiological analysis of pyramidal neurons from control and Dgcr8 conditional knockout mice. Pyramidal neurons in the cortex receive extensive excitatory connections from intralaminar, interlaminar and subcortical afferents. Accordingly, if massive cellular necrosis were occurring, a marked reduction in the frequency of excitatory synaptic events would be predicted. However, our analysis of spontaneous excitatory postsynaptic current (EPSC) recordings from control (*Dgcr8<sup>fl/fl</sup>* n = 11) and Dgcr8 conditional knockout (*Dgcr8<sup>fl/fl</sup>;Cre* n = 16) pyramidal neurons showed similar frequencies of events between genotypes (*Dgcr8<sup>fl/fl</sup>* =  $1.7 \pm 0.1$  Hz; *Dgcr8<sup>fl/fl</sup>;Cre* =  $2.0 \pm 0.5$  Hz;  $p = 0.57$ ; Supplemental Figure 5) indicating that Dgcr8 deletion did not result in a reduced capacity for pyramidal neurons to functionally integrate into excitatory circuitry within the cortex. Interestingly, when we analyzed the shape of isolated EPSC events, we found notable differences between genotypes. EPSC events from Dgcr8 knockouts were larger in amplitude than control (*Dgcr8<sup>fl/fl</sup>* =  $10 \pm 1$  pA; *Dgcr8<sup>fl/fl</sup>;Cre* =  $12 \pm 1$  pA;  $p = 0.03$ ). Also, the kinetics were markedly faster in the knockouts, as both the activation times (event 10–90% rise time: *Dgcr8<sup>fl/fl</sup>* =  $1.2 \pm 0.1$  ms; *Dgcr8<sup>fl/fl</sup>;Cre* =  $0.8 \pm 0.1$  ms;  $p < 0.0001$ ) and decay times (event half-width: *Dgcr8<sup>fl/fl</sup>* =  $8.4 \pm 0.5$  ms; *Dgcr8<sup>fl/fl</sup>;Cre* =  $3.8 \pm 0.5$  ms;  $p < 0.0001$ ) were faster in the Dgcr8 knockout than in the control.

Lastly, we examined the passive electrical properties of control and Dgcr8 conditional knockout pyramidal neurons. As expected for neurons of smaller size, input resistance ( $R_{in}$ ) measured through the I-V plot of whole-cell current responses to a series of 5 mV voltage steps was significantly increased in *Dgcr8<sup>fl/fl</sup>;Cre* neurons compared to control (*Dgcr8<sup>fl/fl</sup>*  $R_{in}$  =  $440 \pm 32$  M $\Omega$ , n = 15 cells; *Dgcr8<sup>fl/fl</sup>;Cre*  $R_{in}$  =  $701 \pm 97$  M $\Omega$ , n = 17 cells,  $p = 0.02$ ; Supplemental Figure 5). Conversely, measurement of the whole-cell capacitance ( $C_c$ ) showed that this value was significantly decreased in *Dgcr8<sup>fl/fl</sup>;Cre* pyramidal neurons (*Dgcr8<sup>fl/fl</sup>*  $C_c$  =  $69 \pm 5$  pF, n = 17 cells; *Dgcr8<sup>fl/fl</sup>;Cre*  $C_c$  =  $36 \pm 2$  pF, n = 17 cells;  $p < 0.0001$ ). Next, we examined the membrane time constants ( $\tau_m$ ) and resting membrane potential of pyramidal neurons.  $\tau_m$  values were determined by the single exponential fit of the time course of the membrane voltage response to a  $-25$  pA current step, and these values were similar between genotypes (*Dgcr8<sup>fl/fl</sup>*  $\tau_m$  =  $48 \pm 4$  ms, n = 16 cells; *Dgcr8<sup>fl/fl</sup>;Cre*  $\tau_m$  =  $39 \pm 5$  ms, n = 17 cells,  $p = 0.22$ ). The resting membrane potential was also not significantly different in the conditional knockout (*Dgcr8<sup>fl/fl</sup>*  $V_m$  =  $68 \pm 2$  mV, n = 10 cells; *Dgcr8<sup>fl/fl</sup>;Cre*  $V_m$  =  $60 \pm 5$  mV, n = 15 cells,  $p = 0.16$ ). Together, these data show that *Dgcr8<sup>fl/fl</sup>;Cre* neurons display altered whole-cell electrical properties consistent with morphological changes, but with no observable changes to specific membrane properties or leak conductances that may be associated with neuronal death.

## 4 Discussion

In this study, we demonstrate a critical role for Dgcr8-dependent miRNA biogenesis in the development of the cytoarchitecture of the cerebral cortex. We find that conditional ablation

of *Dgcr8* in newly-born pyramidal neurons results in profound morphological defects, including microencephaly due to cortical thinning, decreased soma size, and loss of dendritic complexity. These results are largely in agreement with the anatomical findings from postmitotic deletions of *Dicer* (Davis et al., 2008; De Pietri Tonelli et al., 2008; Kawase-Koga et al., 2009); however, we did not observe the grossly disrupted lamination which has consistently been reported across multiple conditional *Dicer* strains (De Pietri Tonelli et al., 2008; Kawase-Koga et al., 2009), suggesting that miRNA-independent pathways may underlie this component of the *Dicer* phenotype. In addition, we performed immunohistological, electrophysiological, and behavioral analyses that have not previously been conducted in *Dicer* models, leading to the identification of a novel effect of miRNAs on inhibitory transmission.

This work is notable as the first molecular- to systems-level characterization of a conditional ablation of *Dgcr8* in the mammalian CNS. As such, this study is the first to explicitly address the impact of miRNA loss in the developing cortex. Loss of other classes of small RNAs may have confounded the results of previous studies in which *Dicer* deletion was used as a measure of miRNA function. Side-by-side deep sequencing of conditional *Dicer* versus *Dgcr8* neuronal knockouts has identified a pool of highly-expressed non-canonical miRNAs that are processed by *Dicer* but not by *Dgcr8*. In addition, the *Dicer* knockout animals exhibited earlier lethality and significant structural abnormalities compared to the *Dgcr8* knockout animals (Babiarz et al., 2011). This is an important issue given that the identity and mechanism of action of other *Dicer*-dependent RNAs is largely unknown, and evidence suggests that their function may be distinct from that of canonical miRNAs. For instance, endo-siRNAs processed by *Dicer* typically result in target degradation, whereas *Dgcr8*-derived miRNAs more commonly act via translational repression (Ambros, 2004; Bartel, 2004). Most recently, *Dicer* has been shown to have a novel miRNA-independent function in processing Alu RNAs, and conditional loss of *Dicer* induces Alu RNA toxicity leading to a macular degeneration phenotype, an effect not observed following loss of *Dgcr8* (Kaneko et al., 2011). Previous studies examining *Dicer*-dependent effects did not analyze Alu RNAs, and it is possible that toxicity induced by Alu RNAs may be a component of these phenotypes (Meister, 2011). To isolate the miRNA pathway, it is therefore critical to characterize a system via depletion of *Dgcr8* rather than *Dicer*.

Our finding that PV interneurons are selectively reduced in the PFC of *Dgcr8<sup>fl/fl</sup>;Cre* mice was unexpected because the Cre recombinase expression is limited to post-mitotic principle neurons of the cortex. This would suggest that elements extrinsic to interneurons, such as trophic factors expressed by principle neurons, might be dysregulated in *Dgcr8<sup>fl/fl</sup>;Cre* mice. BDNF and TrkB are required for the proper maturation of PV interneurons in the cortex (Eto et al., 2010; Patz et al., 2004; Wahle et al., 2000), and loss of activity-dependent BDNF results in reductions in PV expression as well as changes in IPSCs in the mPFC (Sakata et al., 2009). The reductions of both BDNF and TrkB in the PFC of *Dgcr8<sup>fl/fl</sup>;Cre* mice suggests that disrupted signaling through the BDNF/TrkB pathway may be in part responsible for the observed changes in PV expression and inhibitory transmission. miRNAs have been predicted to target BDNF itself; however, brain-specific miRNAs have also been shown to target molecules which regulate BDNF expression, including RE-1 silencing transcription factor (REST) (Conaco et al., 2006; Packer et al., 2008; Wu and Xie, 2006) and methyl CpG-binding protein 2 (MeCP2) (Im et al., 2010; Klein et al., 2007), through homeostatic and double-negative feedback interactions. Furthermore, miRNAs are thought to fine-tune gene expression and are commonly observed in feedforward and feedback loops which serve to maintain neuronal homeostasis (Tsang et al., 2007). Given the pleiotropic effects of BDNF signaling as well as the multiple levels of regulation acting on BDNF, it is likely that the interaction between miRNAs and BDNF expression are complex and interconnected. Decreases in BDNF and TrkB are likely to have many downstream effects,

and alterations in PV interneurons is only one of many possible consequences. Additional studies will be necessary to determine whether the loss of PV expression is directly due to the downregulation of BDNF or to other indirect effects of miRNA loss, as well as to determine the precise mechanism underlying the loss of PV neurons.

The selective reduction of PV interneurons is particularly interesting given that PV is expressed by basket cell interneurons which are known to primarily synapse perisomatically (DeFelipe, 1997; Freund and Katona, 2007; Williams et al., 1992). Accordingly, reductions in this powerful source of inhibition would likely result in hyperexcitability and aberrant network activity, which may underlie some of the severe behavioral deficits observed in *Dgcr8<sup>fl/fl</sup>;Cre* mice. While it is possible that the reduction in perisomatic inhibitory synapses may be in part due to the smaller cell bodies in the *Dgcr8<sup>fl/fl</sup>;Cre*, the change in inhibition is supported by electrophysiological recordings. Specifically, although IPSC frequency was dramatically reduced in pyramidal neurons, we found that the remaining IPSC events were significantly larger in amplitude, a result that was confirmed through mIPSC recordings as attributable to a postsynaptic origin. These results would indicate that despite the loss of miRNA expression, pyramidal neurons are still able to form functional postsynaptic GABA-A receptor complexes. The larger IPSC amplitudes could reflect a compensatory mechanism, such as synaptic scaling, in response to the deficit in perisomatic inhibition.

Our electrophysiological analysis of *Dgcr8<sup>fl/fl</sup>;Cre* pyramidal neurons also indicates that despite their morphogenic defects, these neurons sit hyperpolarized ( $V_m = \sim -60$  mV), display a normal membrane time constant, fire action potentials, and receive excitatory as well as inhibitory synaptic transmission (Supplemental Figure 5). While the elevated levels of cell death we observe could account for the microencephaly and for some of the changes in gross morphology, these physiological properties are not hallmarks of dying neurons, suggesting that the pyramidal neurons that survive are alive, functional and integrated into cortical circuitry. We argue that increased cell death is unlikely to result in a consistent phenotype including decreased IPSC frequency, a specific loss of perisomatic inhibitory synapses, decreases in PV but not CR or SST interneurons, and seizure activity, which together suggest that mechanisms specific to inhibitory transmission are at work. Thus, the loss of a single class of inhibitory neurons (that have normal miRNA expression), while other types of interneurons develop normally, is both unexpected and novel. Together, our data suggest a model in which loss of *Dgcr8* in pyramidal neurons leads to a BDNF-dependent, non-cell-autonomous effect on PV interneuron development. This selective reduction of PV interneurons accounts for the decrease in perisomatic synapses, which in turn, corresponds to the changes in inhibitory transmission.

Finally, our findings have potential implications for understanding the molecular mechanisms underlying human neuropsychiatric disease and illness. Abnormalities in interneuron development and function have been implicated in seizure disorders as well as in autism, anxiety disorders, and schizophrenia (Cobos et al., 2005; Powell et al., 2003; Wonders and Anderson, 2006). Decreases in PV interneurons in the PFC specifically have been described in schizophrenia (Blum and Mann, 2002; Mellios et al., 2009; Zhang and Reynolds, 2002), while changes in miRNA expression patterns have been reported in schizophrenia postmortem studies (Beveridge et al., 2008; Perkins et al., 2007). In addition, *Dgcr8* haploinsufficiency contributes to neurological, behavioral, and anatomical phenotypes of the 22q11 Deletion Syndrome (Schofield et al., 2011; Stark et al., 2008), which has been proposed as a genetic subtype of schizophrenia (Liu et al., 2002). Our findings delineate a novel connection between *Dgcr8*-dependent miRNAs in the cortex and PV neuron maturation, and as such, provide a potential inroad toward a mechanistic understanding of the cellular and molecular changes observed in schizophrenia. However, as human schizophrenia lacks the severe gross cortical malformations observed in

*Dgcr8<sup>fl/fl</sup>;Cre* mice, a more likely scenario is that small-scale changes of specific miRNA levels during postnatal development similar to those observed in the heterozygous *Dgcr8* mice (Fenelon et al., 2011; Schofield et al., 2011), are involved in the emergent phenotypes of schizophrenia, including the changes in PV expression. Identification of individual miRNAs in the cortex mediating such effects will be the basis of future studies.

## Supplementary Material

Refer to Web version on PubMed Central for supplementary material.

## Acknowledgments

Funding for this project was supported in part by the NIH T32EY07120 (RH); NIH R21-MH083090 and Autism Speaks (EMU); and K08 NS48118, R01 NS057221, and California Institute of Regenerative Medicine New Faculty Award RN2-00906 (RB). This work was made possible in part by the NIH-NEI EY002162 Core Grant for Vision Research. The authors are grateful to Tigwa Davis, Selina Koch, Gemma Rooney, Caitlyn Gertz, and Robert Krencik for helpful discussion, critical readings of the manuscript, and technical assistance. We thank Lawrence Sincich and the laboratory of Jonathan Horton for aiding in image acquisition and cell density analyses. We also thank Ryan Sze and Tony Tran for assistance with genotyping and Beth Grande for administrative support.

## References

- Ambros V. The functions of animal microRNAs. *Nature*. 2004; 431:350–5. [PubMed: 15372042]
- Babiarz JE, Ruby JG, Wang Y, Bartel DP, Blelloch R. Mouse ES cells express endogenous shRNAs, siRNAs, and other Microprocessor-independent, Dicer-dependent small RNAs. *Genes Dev*. 2008; 22:2773–85. [PubMed: 18923076]
- Babiarz JE, Hsu R, Melton C, Thomas M, Ullian EM, Blelloch R. A role for non-canonical microRNAs in the mammalian brain revealed by phenotypic differences in *Dgcr8* versus *Dicer1* knockouts and small RNA sequencing. *RNA*. 2011 In press.
- Bartel DP. MicroRNAs: genomics, biogenesis, mechanism, and function. *Cell*. 2004; 116:281–97. [PubMed: 14744438]
- Beveridge NJ, Tooney PA, Carroll AP, Gardiner E, Bowden N, Scott RJ, Tran N, Dedova I, Cairns MJ. Dysregulation of miRNA 181b in the temporal cortex in schizophrenia. *Hum Mol Genet*. 2008; 17:1156–68. [PubMed: 18184693]
- Blum BP, Mann JJ. The GABAergic system in schizophrenia. *Int J Neuropsychopharmacol*. 2002; 5:159–79. [PubMed: 12135541]
- Cao X, Yeo G, Muotri AR, Kuwabara T, Gage FH. Noncoding RNAs in the mammalian central nervous system. *Annu Rev Neurosci*. 2006; 29:77–103. [PubMed: 16776580]
- Chiu CS, Brickley S, Jensen K, Southwell A, McKinney S, Cull-Candy S, Mody I, Lester HA. GABA transporter deficiency causes tremor, ataxia, nervousness, and increased GABA-induced tonic conductance in cerebellum. *J Neurosci*. 2005; 25:3234–45. [PubMed: 15788781]
- Cobos I, Calcagno ME, Vilaythong AJ, Thwin MT, Noebels JL, Baraban SC, Rubenstein JL. Mice lacking *Dlx1* show subtype-specific loss of interneurons, reduced inhibition and epilepsy. *Nat Neurosci*. 2005; 8:1059–68. [PubMed: 16007083]
- Conaco C, Otto S, Han JJ, Mandel G. Reciprocal actions of REST and a microRNA promote neuronal identity. *Proc Natl Acad Sci U S A*. 2006; 103:2422–7. [PubMed: 16461918]
- Davis TH, Cuellar TL, Koch SM, Barker AJ, Harfe BD, McManus MT, Ullian EM. Conditional loss of *Dicer* disrupts cellular and tissue morphogenesis in the cortex and hippocampus. *J Neurosci*. 2008; 28:4322–30. [PubMed: 18434510]
- De Pietri Tonelli D, Pulvers JN, Haffner C, Murchison EP, Hannon GJ, Huttner WB. miRNAs are essential for survival and differentiation of newborn neurons but not for expansion of neural progenitors during early neurogenesis in the mouse embryonic neocortex. *Development*. 2008; 135:3911–21. [PubMed: 18997113]

- DeFelipe J. Types of neurons, synaptic connections and chemical characteristics of cells immunoreactive for calbindin-D28K, parvalbumin and calretinin in the neocortex. *J Chem Neuroanat.* 1997; 14:1–19. [PubMed: 9498163]
- Eto R, Abe M, Kimoto H, Imaoka E, Kato H, Kasahara J, Araki T. Alterations of interneurons in the striatum and frontal cortex of mice during postnatal development. *Int J Dev Neurosci.* 2010; 28:359–70. [PubMed: 20406674]
- Fenelon K, Mukai J, Xu B, Hsu PK, Drew LJ, Karayiorgou M, Fischbach GD, Macdermott AB, Gogos JA. Deficiency of *Dgcr8*, a gene disrupted by the 22q11.2 microdeletion, results in altered short-term plasticity in the prefrontal cortex. *Proc Natl Acad Sci U S A.* 2011; 108:4447–52. [PubMed: 21368174]
- Freund TF, Katona I. Perisomatic inhibition. *Neuron.* 2007; 56:33–42. [PubMed: 17920013]
- Goebbels S, Bormuth I, Bode U, Hermanson O, Schwab MH, Nave KA. Genetic targeting of principal neurons in neocortex and hippocampus of NEX-Cre mice. *Genesis.* 2006; 44:611–21. [PubMed: 17146780]
- Im HI, Hollander JA, Bali P, Kenny PJ. MeCP2 controls BDNF expression and cocaine intake through homeostatic interactions with microRNA-212. *Nat Neurosci.* 2010; 13:1120–7. [PubMed: 20711185]
- Kaneko H, Dridi S, Tarallo V, Gelfand BD, Fowler BJ, Cho WG, Kleinman ME, Ponicsan SL, Hauswirth WW, Chiodo VA, Kariko K, Yoo JW, Lee DK, Hadziahmetovic M, Song Y, Misra S, Chaudhuri G, Buas FW, Braun RE, Hinton DR, Zhang Q, Grossniklaus HE, Provis JM, Madigan MC, Milam AH, Justice NL, Albuquerque RJ, Blandford AD, Bogdanovich S, Hirano Y, Witta J, Fuchs E, Littman DR, Ambati BK, Rudin CM, Chong MM, Provost P, Kugel JF, Goodrich JA, Dunaief JL, Baffi JZ, Ambati J. DICER1 deficit induces Alu RNA toxicity in age-related macular degeneration. *Nature.* 2011; 471:325–30. [PubMed: 21297615]
- Kawase-Koga Y, Otaegi G, Sun T. Different timings of Dicer deletion affect neurogenesis and gliogenesis in the developing mouse central nervous system. *Dev Dyn.* 2009; 238:2800–12. [PubMed: 19806666]
- Kiernan, JA. *Histological and histochemical methods: theory and practice.* 2. Pergamon; 1990.
- Kim VN. Small RNAs: classification, biogenesis, and function. *Mol Cells.* 2005; 19:1–15. [PubMed: 15750334]
- Klein ME, Lioy DT, Ma L, Impy S, Mandel G, Goodman RH. Homeostatic regulation of MeCP2 expression by a CREB-induced microRNA. *Nat Neurosci.* 2007; 10:1513–4. [PubMed: 17994015]
- Liu H, Abecasis GR, Heath SC, Knowles A, Demars S, Chen YJ, Roos JL, Rapoport JL, Gogos JA, Karayiorgou M. Genetic variation in the 22q11 locus and susceptibility to schizophrenia. *Proc Natl Acad Sci U S A.* 2002; 99:16859–64. [PubMed: 12477929]
- Markram H, Toledo-Rodriguez M, Wang Y, Gupta A, Silberberg G, Wu C. Interneurons of the neocortical inhibitory system. *Nat Rev Neurosci.* 2004; 5:793–807. [PubMed: 15378039]
- Meister G. Vision: Dicer leaps into view. *Nature.* 2011; 471:308–9. [PubMed: 21412326]
- Mellios N, Huang HS, Baker SP, Galdzicka M, Ginns E, Akbarian S. Molecular determinants of dysregulated GABAergic gene expression in the prefrontal cortex of subjects with schizophrenia. *Biol Psychiatry.* 2009; 65:1006–14. [PubMed: 19121517]
- Miles R, Toth K, Gulyas AI, Hajos N, Freund TF. Differences between somatic and dendritic inhibition in the hippocampus. *Neuron.* 1996; 16:815–23. [PubMed: 8607999]
- Packer AN, Xing Y, Harper SQ, Jones L, Davidson BL. The bifunctional microRNA miR-9/miR-9\* regulates REST and CoREST and is downregulated in Huntington's disease. *J Neurosci.* 2008; 28:14341–6. [PubMed: 19118166]
- Patz S, Grabert J, Gorba T, Wirth MJ, Wahle P. Parvalbumin expression in visual cortical interneurons depends on neuronal activity and TrkB ligands during an Early period of postnatal development. *Cereb Cortex.* 2004; 14:342–51. [PubMed: 14754872]
- Perkins DO, Jeffries CD, Jarskog LF, Thomson JM, Woods K, Newman MA, Parker JS, Jin J, Hammond SM. microRNA expression in the prefrontal cortex of individuals with schizophrenia and schizoaffective disorder. *Genome Biol.* 2007; 8:R27. [PubMed: 17326821]
- Pfaffl MW. A new mathematical model for relative quantification in real-time RT-PCR. *Nucleic Acids Res.* 2001; 29:e45. [PubMed: 11328886]

- Powell EM, Campbell DB, Stanwood GD, Davis C, Noebels JL, Levitt P. Genetic disruption of cortical interneuron development causes region- and GABA cell type-specific deficits, epilepsy, and behavioral dysfunction. *J Neurosci*. 2003; 23:622–31. [PubMed: 12533622]
- Racine RJ. Modification of seizure activity by electrical stimulation. II. Motor seizure. *Electroencephalogr Clin Neurophysiol*. 1972; 32:281–94. [PubMed: 4110397]
- Rao PK, Toyama Y, Chiang HR, Gupta S, Bauer M, Medvid R, Reinhardt F, Liao R, Krieger M, Jaenisch R, Lodish HF, Blalock R. Loss of cardiac microRNA-mediated regulation leads to dilated cardiomyopathy and heart failure. *Circ Res*. 2009; 105:585–94. [PubMed: 19679836]
- Sakata K, Woo NH, Martinowich K, Greene JS, Schloesser RJ, Shen L, Lu B. Critical role of promoter IV-driven BDNF transcription in GABAergic transmission and synaptic plasticity in the prefrontal cortex. *Proc Natl Acad Sci U S A*. 2009; 106:5942–7. [PubMed: 19293383]
- Schofield CM, Hsu R, Barker AJ, Gertz CC, Blalock R, Ullian EM. Monoallelic deletion of the microRNA biogenesis gene *Dgcr8* produces deficits in the development of excitatory synaptic transmission in the prefrontal cortex. *Neural Dev*. 2011; 6:11. [PubMed: 21466685]
- Shapiro JS, Varble A, Pham AM, Tenoever BR. Noncanonical cytoplasmic processing of viral microRNAs. *RNA*. 2010; 16:2068–74. [PubMed: 20841420]
- Stark KL, Xu B, Bagchi A, Lai WS, Liu H, Hsu R, Wan X, Pavlidis P, Mills AA, Karayiorgou M, Gogos JA. Altered brain microRNA biogenesis contributes to phenotypic deficits in a 22q11-deletion mouse model. *Nat Genet*. 2008; 40:751–60. [PubMed: 18469815]
- Tang F, Hajkova P, Barton SC, Lao K, Surani MA. MicroRNA expression profiling of single whole embryonic stem cells. *Nucleic Acids Res*. 2006; 34:e9. [PubMed: 16434699]
- Tsang J, Zhu J, van Oudenaarden A. MicroRNA-mediated feedback and feedforward loops are recurrent network motifs in mammals. *Mol Cell*. 2007; 26:753–67. [PubMed: 17560377]
- Wahle P, Gorba T, Wirth MJ, Obst-Pernberg K. Specification of neuropeptide Y phenotype in visual cortical neurons by leukemia inhibitory factor. *Development*. 2000; 127:1943–51. [PubMed: 10751182]
- Wang Y, Medvid R, Melton C, Jaenisch R, Blalock R. DGCR8 is essential for microRNA biogenesis and silencing of embryonic stem cell self-renewal. *Nat Genet*. 2007; 39:380–5. [PubMed: 17259983]
- Williams SM, Goldman-Rakic PS, Leranth C. The synaptology of parvalbumin-immunoreactive neurons in the primate prefrontal cortex. *J Comp Neurol*. 1992; 320:353–69. [PubMed: 1613130]
- Wonders CP, Anderson SA. The origin and specification of cortical interneurons. *Nat Rev Neurosci*. 2006; 7:687–96. [PubMed: 16883309]
- Wu H, Xu H, Miraglia LJ, Croke ST. Human RNase III is a 160-kDa protein involved in preribosomal RNA processing. *J Biol Chem*. 2000; 275:36957–65. [PubMed: 10948199]
- Wu J, Xie X. Comparative sequence analysis reveals an intricate network among REST, CREB and miRNA in mediating neuronal gene expression. *Genome Biol*. 2006; 7:R85. [PubMed: 17002790]
- Zhang ZJ, Reynolds GP. A selective decrease in the relative density of parvalbumin-immunoreactive neurons in the hippocampus in schizophrenia. *Schizophr Res*. 2002; 55:1–10. [PubMed: 11955958]
- Zhou XF, Rush RA. Endogenous brain-derived neurotrophic factor is anterogradely transported in primary sensory neurons. *Neuroscience*. 1996; 74:945–53. [PubMed: 8895863]

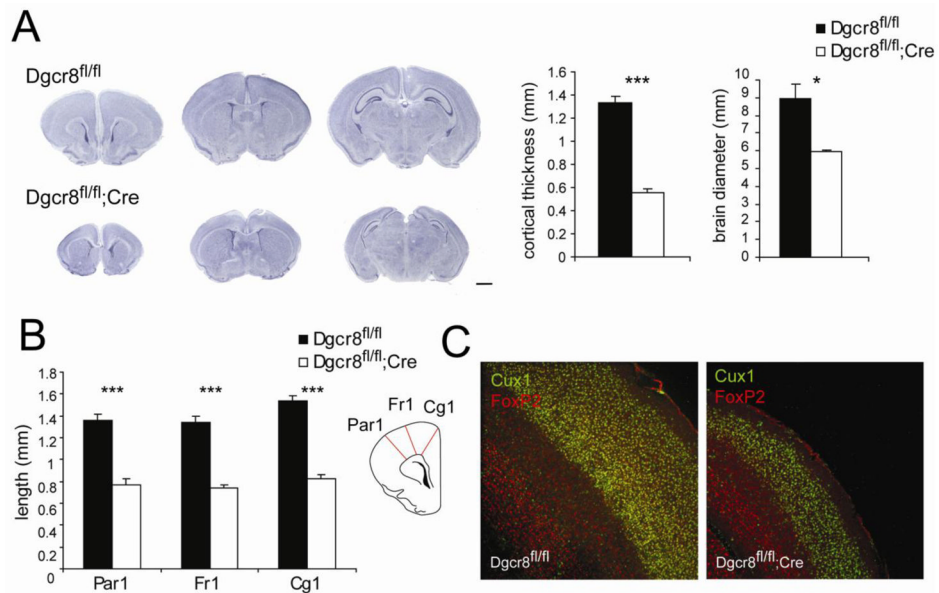


**Figure 1. Gross anatomical phenotypes of *Dgcr8*<sup>fl/fl</sup> vs *Dgcr8*<sup>fl/fl</sup>;Cre mice**

(A) Nissl staining showing microencephaly of the *Dgcr8*<sup>fl/fl</sup>;Cre brain. Scale bar = 1 mm. Quantification reflects reduced cortical thickness and brain diameter in the conditional *Dgcr8*<sup>fl/fl</sup>;Cre. (B) Nissl staining quantification shows reduced PFC measurements in the *Dgcr8*<sup>fl/fl</sup>;Cre. (C) Immunostaining for the upper layer marker Cux1 (green) and the deeper layer marker FoxP2 (red) demonstrated that overall cortical positional identities for these markers were retained in *Dgcr8*<sup>fl/fl</sup>;Cre animals. Error bars represent SEM.

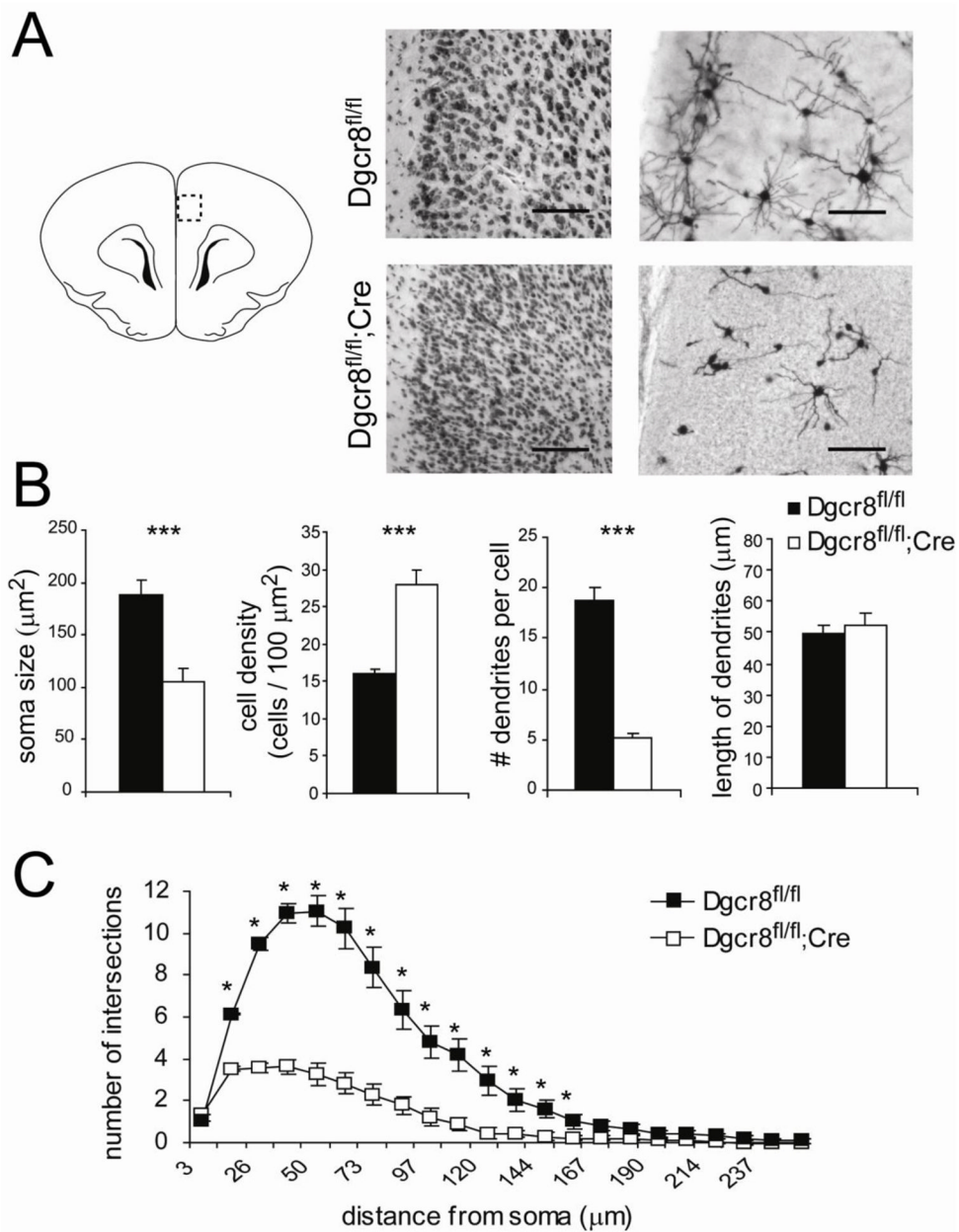


**Figure 2. Reduced soma size and dendritic elaboration in the cortex of the *Dgcr8<sup>fl/fl</sup>;Cre***  
 (A) Cellular quantification in the medial PFC region of *Dgcr8<sup>fl/fl</sup>* under 10x Nissl (left) and 10x Golgi staining (right). Scale bars = 0.1 mm. (B) Soma size is reduced, cell density is increased, and the number of dendrites per cell is significantly reduced in the *Dgcr8<sup>fl/fl</sup>;Cre*. However, the average dendritic length is unchanged. (C) Sholl analysis of mPFC pyramidal neurons reflects reduced dendritic elaboration in the *Dgcr8<sup>fl/fl</sup>;Cre*. Error bars represent SEM.

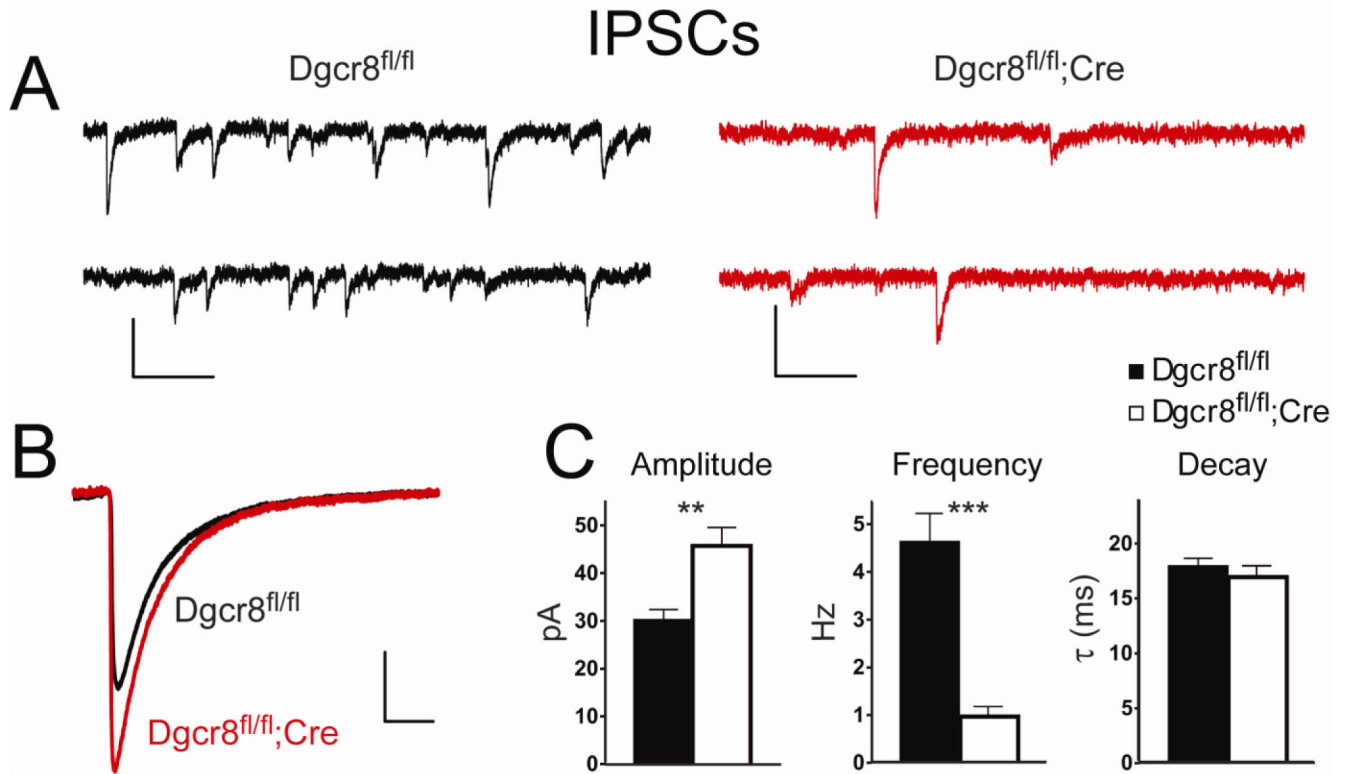


**Figure 3. Altered inhibitory synaptic transmission in pyramidal neurons in the *Dgcr8* conditional knockout cortex**

Representative IPSC recordings from layer II/III pyramidal neurons from *Dgcr8<sup>fl/fl</sup>* and *Dgcr8<sup>fl/fl</sup>;Cre* mice. Scale bar = 50 pA, 200 ms. (B) Mean IPSC responses (average of >50 isolated events) from individual *Dgcr8<sup>fl/fl</sup>* (black) and *Dgcr8<sup>fl/fl</sup>;Cre* (red) neurons superimposed on the same scale illustrate the gain in amplitude with no changes to IPSC kinetics. (C) Summary of IPSC parameters from *Dgcr8<sup>fl/fl</sup>* (n = 13) and *Dgcr8<sup>fl/fl</sup>;Cre* (n = 13) neurons demonstrate a statically significant decrease in frequency and increase in amplitude. The biexponential decay time ( $\tau$ ) was unaltered. Error bars represent SEM.

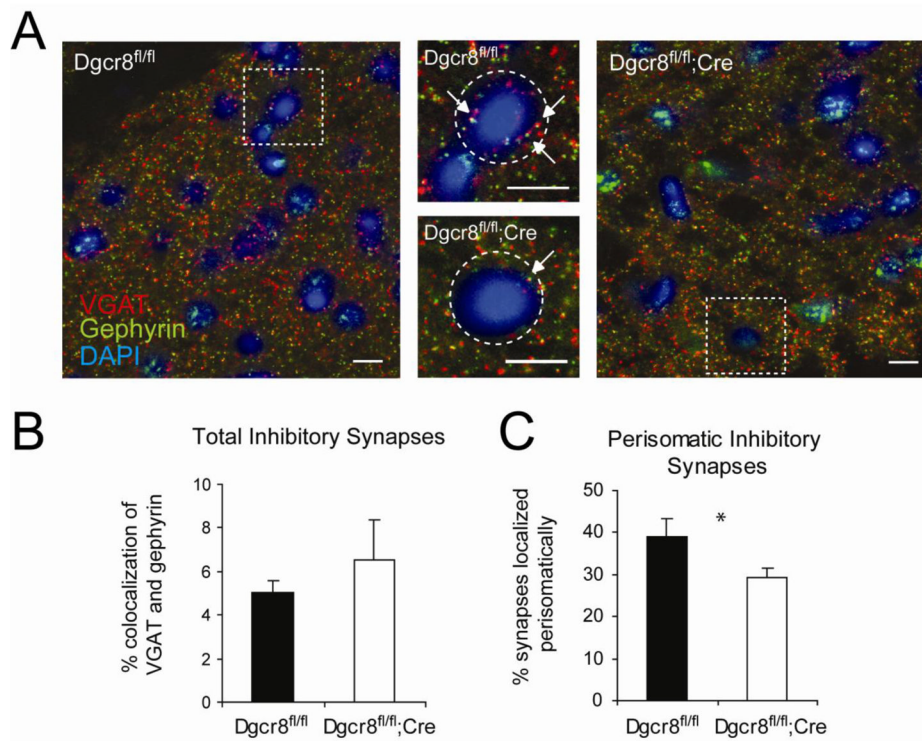


**Figure 4. Immunostaining of inhibitory synapses in the PFC**

(A) VGAT (red), gephyrin (green), and DAPI (blue) staining taken at 63x. Scale bars on all images = 10  $\mu$ m. Arrows indicate colocalization of VGAT and gephyrin signal within the perisomatic space. (B) Quantification of VGAT and gephyrin colocalization as a measure of total inhibitory synapses in the PFC. (C) Percentage of colocalized signal that was located perisomatically, reflecting a reduction in perisomatic inhibitory synapses in the *Dgcr8<sup>fl/fl</sup>;Cre* PFC. Error bars represent SEM.

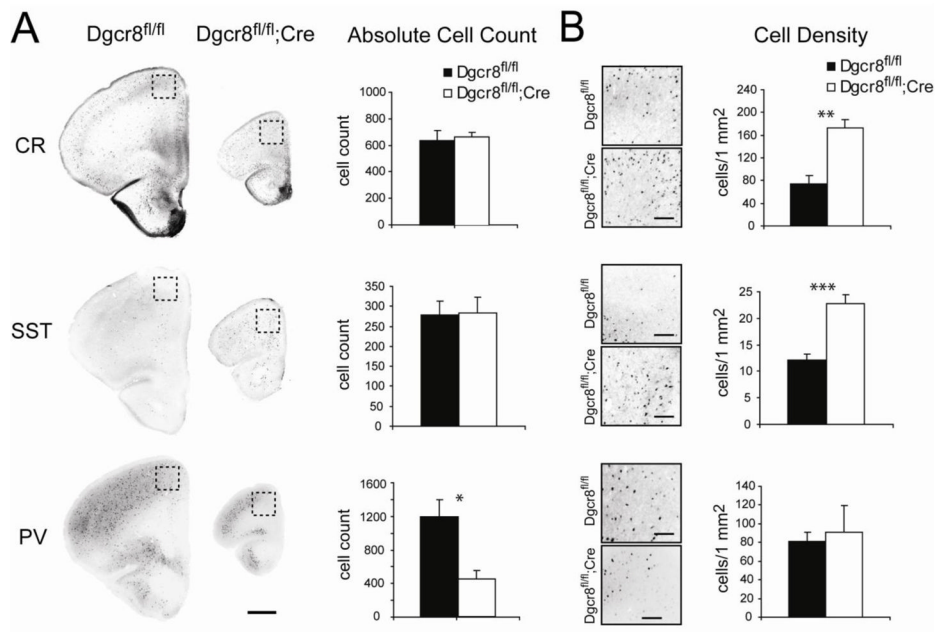


**Figure 5. *Dgcr8<sup>fl/fl</sup>;Cre* animals show a selective reduction of parvalbumin inhibitory interneurons in the PFC**

(A) Representative images showing calretinin (CR), somatostatin (SST), and parvalbumin (PV) immunostaining in the PFC. Scale bar = 1 mm. Quantification of the absolute number of labeled cells in a coronal plane at Bregma 1.545 illustrates a significant reduction in PV cells in the conditional *Dgcr8<sup>fl/fl</sup>;Cre*. (B) Cell density of CR, SST, and PV neurons in the same coronal plane. Scale bar = 0.25 mm. Error bars represent SEM.

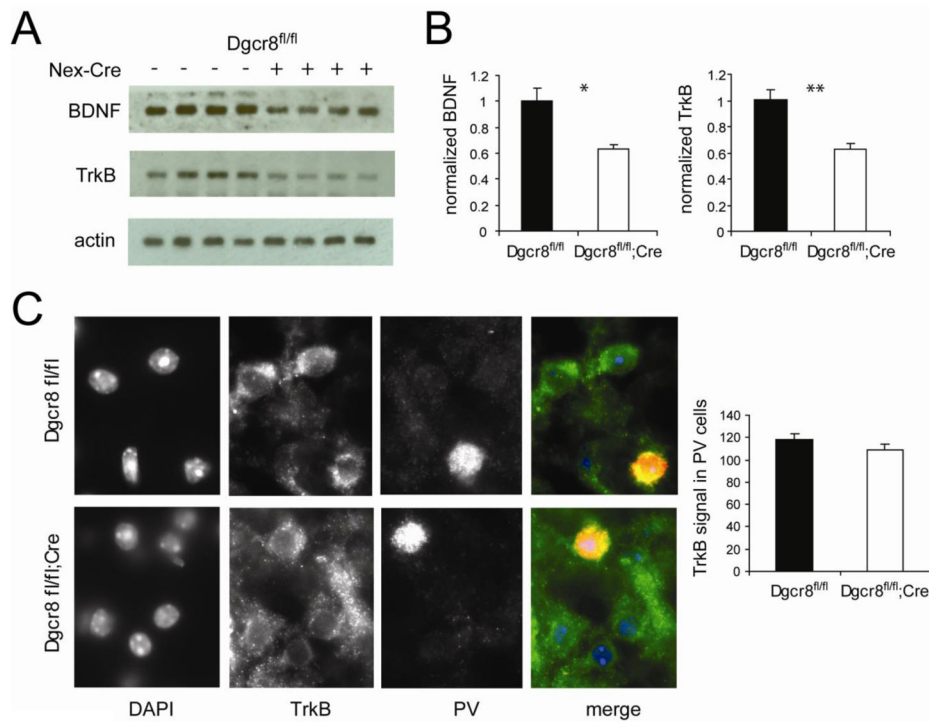


**Figure 6. Reduced BDNF and TrkB protein levels in the *Dgcr8<sup>fl/fl</sup>; Cre***  
 (A) Western blots from total PFC lysates from *Dgcr8<sup>fl/fl</sup>* and *Dgcr8<sup>fl/fl</sup>; Cre* animals. Each lane represents one animal. (B) Quantification of BDNF and TrkB band intensities normalized to actin. (C) Co-staining of TrkB and PV, showing similar levels of TrkB expression in PV-positive cells. Error bars represent SEM.